Conformational Dynamics of the Human Propeller Telomeric DNA Quadruplex on a Microsecond Time Scale

Barira Islam, Miriam Sgobba, Charlie Laughton, Modesto Orozco, Jiri Sponer, Stephen Neidle and Shozeb Haider*

SUPPLEMENTARY DATA

*To whom correspondence should be addressed.

Tel: +442890975806 Fax: +4490972776; Email: s.haider@qub.ac.uk

Conformation of the G-quartet stem

The central core stacking geometry of three G-quartets per complete "helical" turn is retained, as observed in other intramolecular parallel stranded G-quadruplex crystal structures, is maintained throughout the course of the simulation. The G-quadruplex adopts a slightly underwound state when compared to B-form (10.5 bases/turn) and A-form (11 bases/turn) DNA (22). Small variations in geometry are observed in the G-quartet stem, throughout the trajectory when compared with the crystal structure (Table S1). The average distance for N7…N2 and O6…N1 lengthen by 0.2 Å and 0.14 Å to 3.02 Å and 3.0 Å respectively. A slight variation in groove width is observed between the four grooves and shows dependency on the presence or lack of the TTA linkage but not to changes in the TTA loop conformation. The average phosphate-phosphate distance between adjacent strands varies between 14.1-14.9 Å. The grooves expand by ~2 Å when the TTA loop is present and by ~3 Å when it is absent. This dependency of groove expansion to comparable width is a result of expanding G-quartets, which are slightly restricted when the loops are present. A similar breathing effect is observed when ions move through the quadruplex (19), although in our simulations no movement of ions was observed. The average distance between C1' of the top guanine and C1' of the diagonally opposite guanine in the bottom quartet is 9.8 Å. The average distance between adjacent phosphates along the strand is 6.5 Å.

Sugar Pucker and the Backbone Angles

Adenine 1: Ade1 adopts a unique conformation as it flips over and caps the quadruplex for the entire simulation time. The flipping is mediated by a change in the χ angle of Ade1 from an *anti* to a *syn* conformation within the first ns of the production run. We observe that at approximately 470 ns the orientation of the sugar changes so that the χ angle is again in the anti conformation. The position of the base swings back and forth between *anti→syn* positions relative to the base over the later course of the simulation (Figure 3a). The sugar pucker remains in the C2'-*endo* conformation. The ε/ζ crankshaft motions of Ade1 ensure that the nucleotide remains in the conventional B_I conformation.

Quartet 1: The bases Gua2, Gua8, Gua14 and Gua20 constitute the first quartet. The χ angle of all the bases in the quartet 1 lies in a low-energy *anti*-conformation. The sugars in this quartet prefer to adopt a C2'-*endo* pucker. These nucleotides remain in a B_I conformation. In Gua2, Gua8 and Gua14, α/γ crankshaft motions deviate from canonical g-/g+ to non-canonical g+/g+, g+/t and g-/t conformations (Figure S2). This could also be a consequence of conformational changes in Ade1 by a nearest-neighbour effect (40). The conformation change is in concordance with the presence of flexible upstream adenines, Ade1, Ade7 and Ade19. However, Ade13 shows less flexibility and therefore the α/γ backbone combinations of Gua14 prefer to be in canonical g-/g+ conformation region for the entire simulation time.

Quartet 2: The bases Gua3, Gua9, Gua15 and Gua21 constitute the middle quartet. Analysis of the present 1.5 μs simulation suggests that the backbone of quartet 2 is highly flexible. The χ angles of all the nucleotides in the quartets are in an *anti* conformation region. However, Gua15 deviates by ~30° from the quartet plane due to spatial constraints when Thy17 interacts with the G-quartet. The α/γ crankshaft motions predominantly lie in the lowest energy regions of the g-/g+ conformation. The nucleotides occasionally change α/γ angles to a g-/t conformation during the simulation. This occurs in a concerted way and the global geometry of the quartet is not affected. The (ε-ζ) values suggest that while the other guanine bases (Gua3, Gua9 and Gua21) adopt a B_{II} conformation up to a maximum 15% time duration, Gua15 stays in the B_{II} conformation for ~88% of the total simulation time (Figure S3). A plausible explanation is that the groove between Gua15 and Gua21 widens to allow Thy17 to interact with Gua15.

Quartet 3: The third G-quartet in the core is the most stable sub-segment of the quadruplex. The bases Gua4, Gua10 and Gua16 show α/γ crankshaft motions in g-/g+ regions. Gua22 showed slight variations in the α/γ crankshaft motions, which does not affect the global geometry of the quadruplex. The flexibility of Gua22 could be due to a tail effect as it is the terminal base of the structure (Figure S4).

Loop1: The first loop of the quadruplex shows multiple interactions with other bases. This is depicted by large variations in the backbone torsion angles and sugar puckering. The χ angle is *anti* for Thy5 and Thy6 while Ade7 occupies both *syn* and *anti* conformations. The χ angle of Ade7 changes to a *syn* value between 600-900 ns (Figure S6). It is apparent from the trajectory that this change occurs when Ade7 flips over to interact with Ade1 and Ade13, forming a hydrogen-bonded triad. As the triad and backbone interactions last for nearly 300 ns, the χ angle then moves back to an *anti* value. The predominant sugar puckering mode is C2'-*endo* for all the three nucleotides. However when the χ angle of Ade7 is in a *syn* conformation, the sugar pucker of Ade7 shifts to the C1'-*exo* region and that of Thy6 changes to C3'-*endo*. The α/γ torsion angles sample g-/g+, t/g+, g+/g+, g+/t and g-/g- regions, implying that loop1 is highly flexible (Figure S6b). Thy5 adopts a B_{II} conformation for ~15% of the simulation time. However, Ade7 adopts a B_{II} conformation for ~70% of the time (Figure 6c).

Loop2: The second loop of the quadruplex is comparatively more stable than the first one. Thy11 adopts a predominantly *syn* conformation after 500 ns to form a π-stack with Thy12. Thy12 and Ade13 show favorable *anti* glycosidic χ-angles. The puckering mode for sugars associated with all the bases was observed to be C2'-*endo*. All the three nucleotides adopt a predominantly B_I conformation. The α/γ angles for Thy11 and Ade13 are equivalent and lie in non-canonical region of g+/g+ and g-/t. The α/γ angle for Thy12 however clearly lies in canonical g-/g regions (Figure S7).

Loop3: The χ angles of Thy17 and Ade19 have *anti* values while the χ angle of Thy18 occupy both *anti* and *syn* regions (Figure S8). Thy18 and Ade19 show C2'-*endo* puckering

while Thy17 adopts C3'-*endo* pucker (Figure S9). All the three nucleotides adopt B_I backbone conformation. The α/γ angles for Thy17 and Ade19 occupy canonical regions while Thy18 is highly flexible (Figure S8a). The sampling of sugar puckers (Thy17) and backbone parameters (Thy18) in non-canonical regions facilitates interaction of Thy17 with the middle G-quartet of the core as well as π-stacking interactions between Thy18 and Ade19.

	X-ray	**Simulation**
	12 Guanines/turn	12 Guanines/turn
Av. Distance N2-N7	2.82 Å	3.02 Å
Av. Distance O6-N1	2.90 Å	3.04 Å
Av. Phosphate-Phosphate	11.5 Å.- 12.3 Å	14.1 Å -14.9 Å
Av distance C1'-C1'	11.4 Å	11.8 Å

Table S1: Comparison of the general parameters between the starting Xray structure (PDB id 1KF1) and the simulated structure at the end of 1500 ns. The average phosphate-phosphate distance varies by ~3.0 Å and depends upon the presence of loops in the groove.

Color of the cluster	Sampling in the trajectory (%)
Black	46.83
Green	23.72
Orange	16.06
Brown	9.38
Blue	2.61
Red	1.38

Table S2: Clustering analysis showing percentage of different clusters in the trajectory.

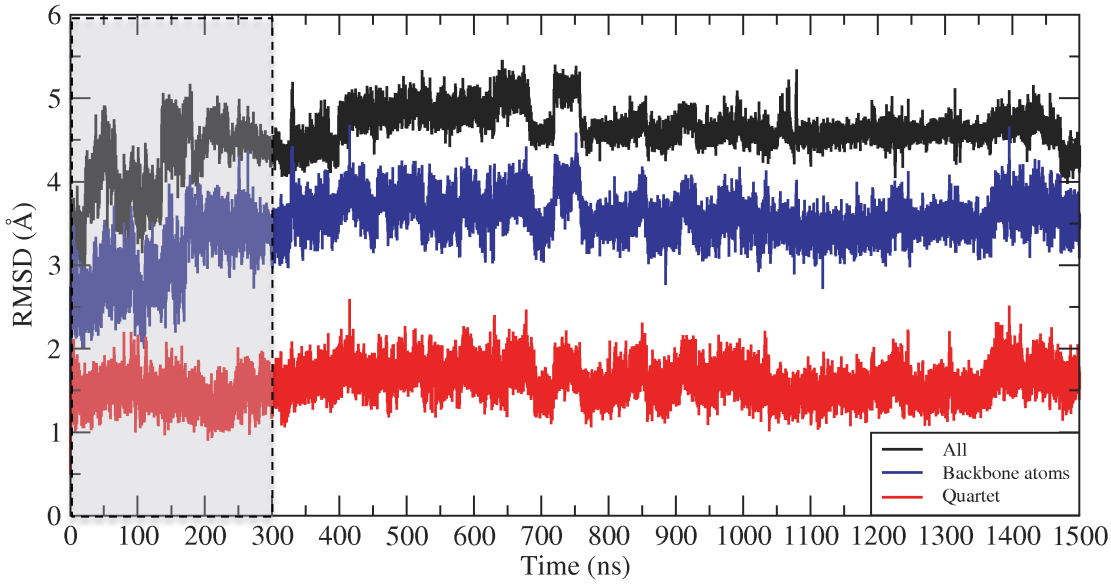

Figure S1: RMSD comparison between different segments of the quadruplex during the simulation. The all atom RMSD of quadruplex is high due to the mobility of the loops, which can be attributed to the wobbling of bases. The quartets are the most stable region of the quadruplex (red). The dashed lines at 300ns demarkate the equilibration cut-off time.

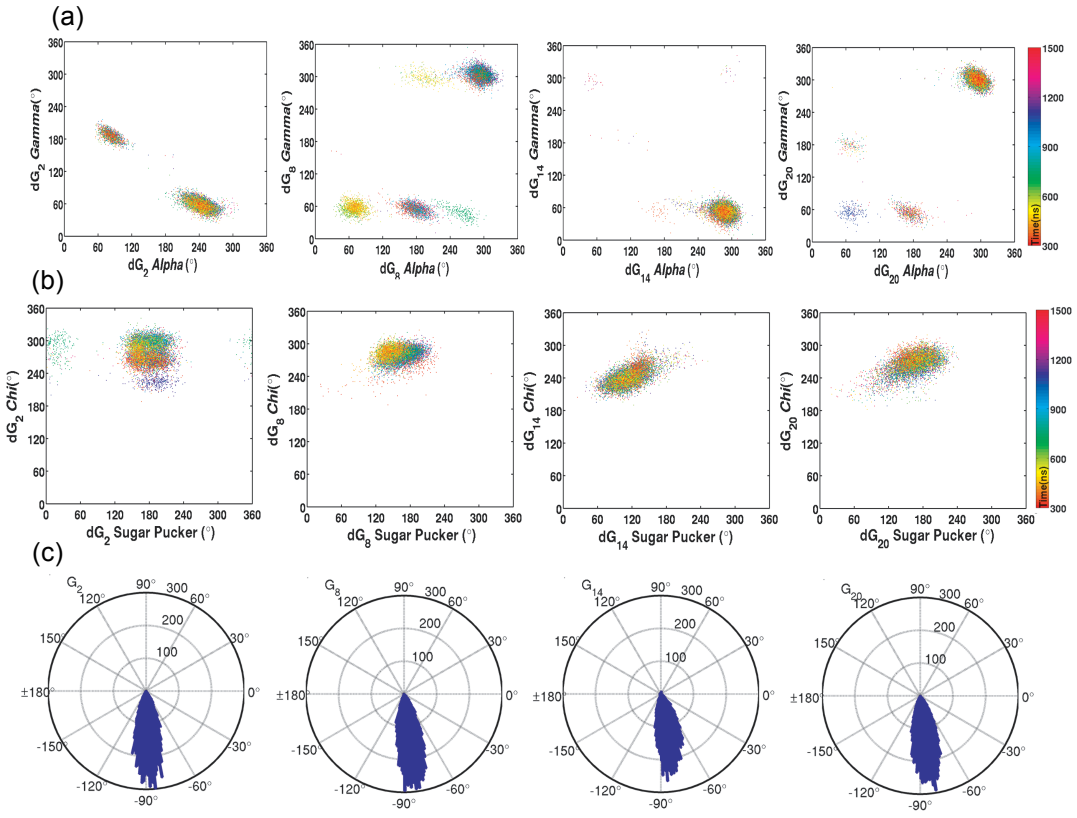

Figure S2: The backbone parameters and sugar pucker angle for first quartet (Gua2, Gua8, Gua 14 and Gua20). The sampling time of **(a)** The α/γ torsion angles and **(b)** χ vs pucker is indicated by color bar. α/γ angles of Gua8 and Gua 20 lie in non-canonical regions due to flexible upstream adenines, Ade7 and Ade19. The sugar pucker of all guanines in quartet1 lie in C2'-*endo* region **(c)** Angular histogram of B_I/B_{II} parameters. The circular lines indicate the sampling frequency in the histogram. The guanines of quartet 1 lie absolutely in B_I conformation.

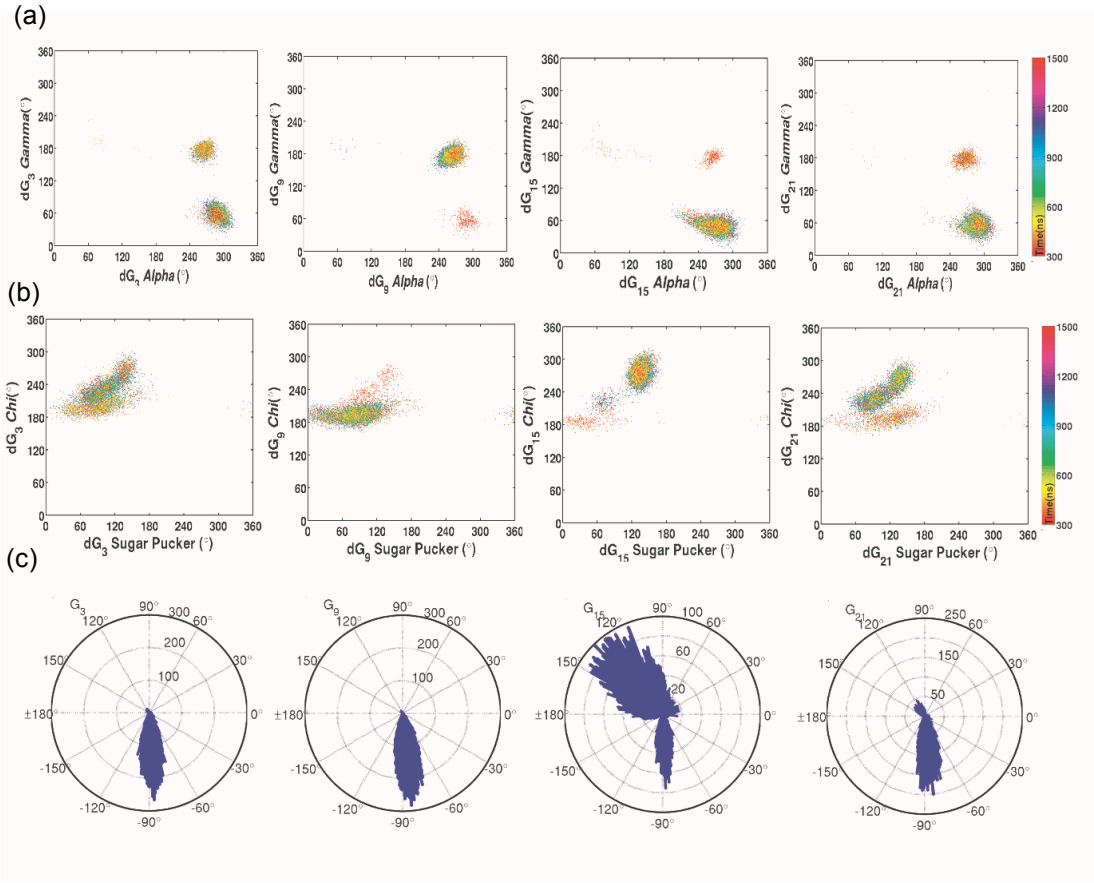

Figure S3: Representations of **(a)** The α/γ torsion angle **(b)** χ vs pucker and **(c)** Angular histogram of B_I/B_{II} parameter of second quartet (Gua3, Gua9, Gua15 and Gua21). While the Gua3 and Gua9 remain mostly in B_I conformation, Gua15 (xx%) and Gua21 (xx%) show occupancy in B_{II} conformation.

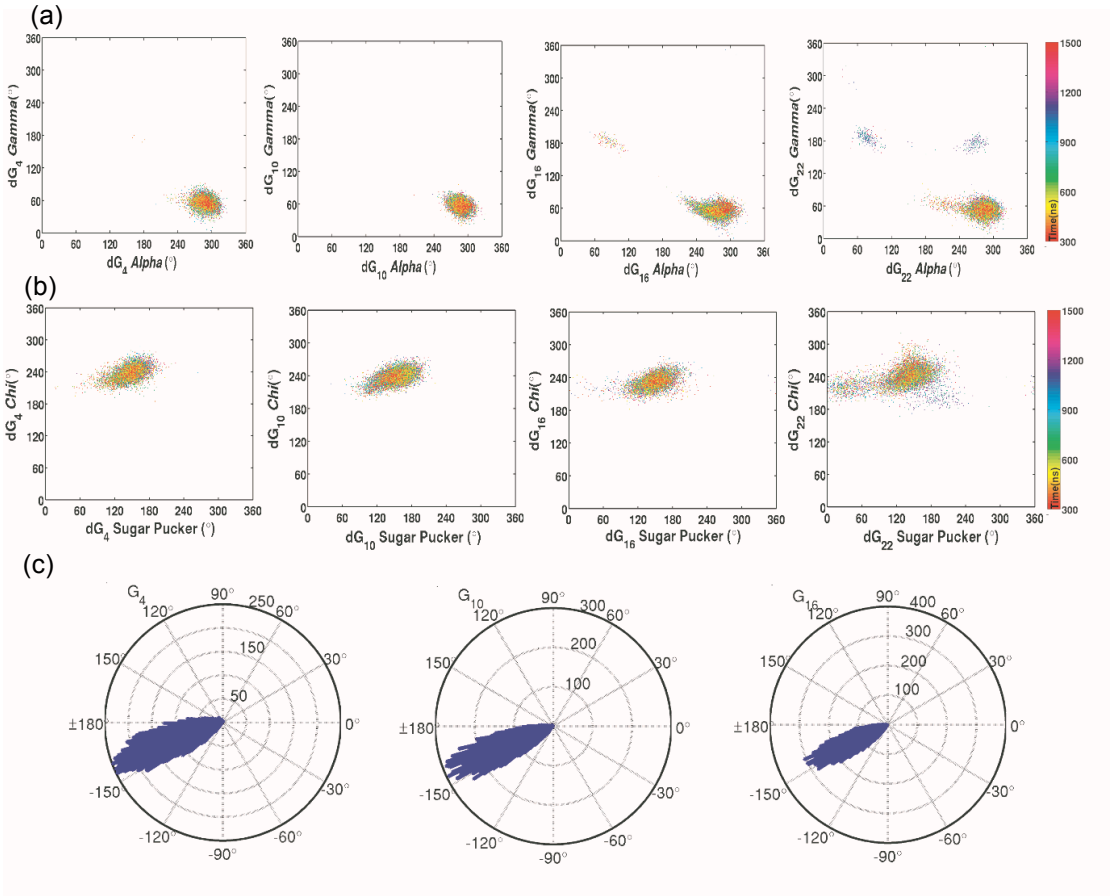

Figure S4: Representation of **(a)** The α/γ torsion angle **(b)** χ vs pucker and **(c)** Angular histogram of B_I/B_{II} parameter of third quartet (Gua4, Gua10, Gua16 and Gua22). The α/γ angle and the puckering of Gua22 shows some flexibility, as it is the terminal base in the quadruplex. The B_I/B_{II} parameters for Gua22 cannot be calculated due to the lack of ε/ζ angles.

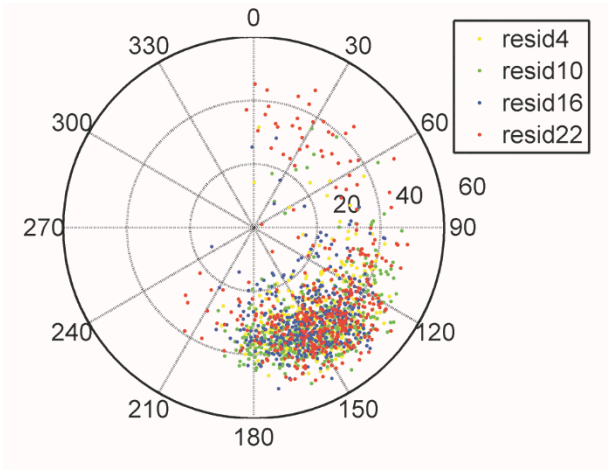

Figure: S5: Polar plot of sugar puckering of third quartet. The sugar pucker of all the bases predominantly lie in C2'-*endo* conformation. Gua22 shows flexible sugar puckering and can be reasoned as it is the terminal base in the quadruplex.

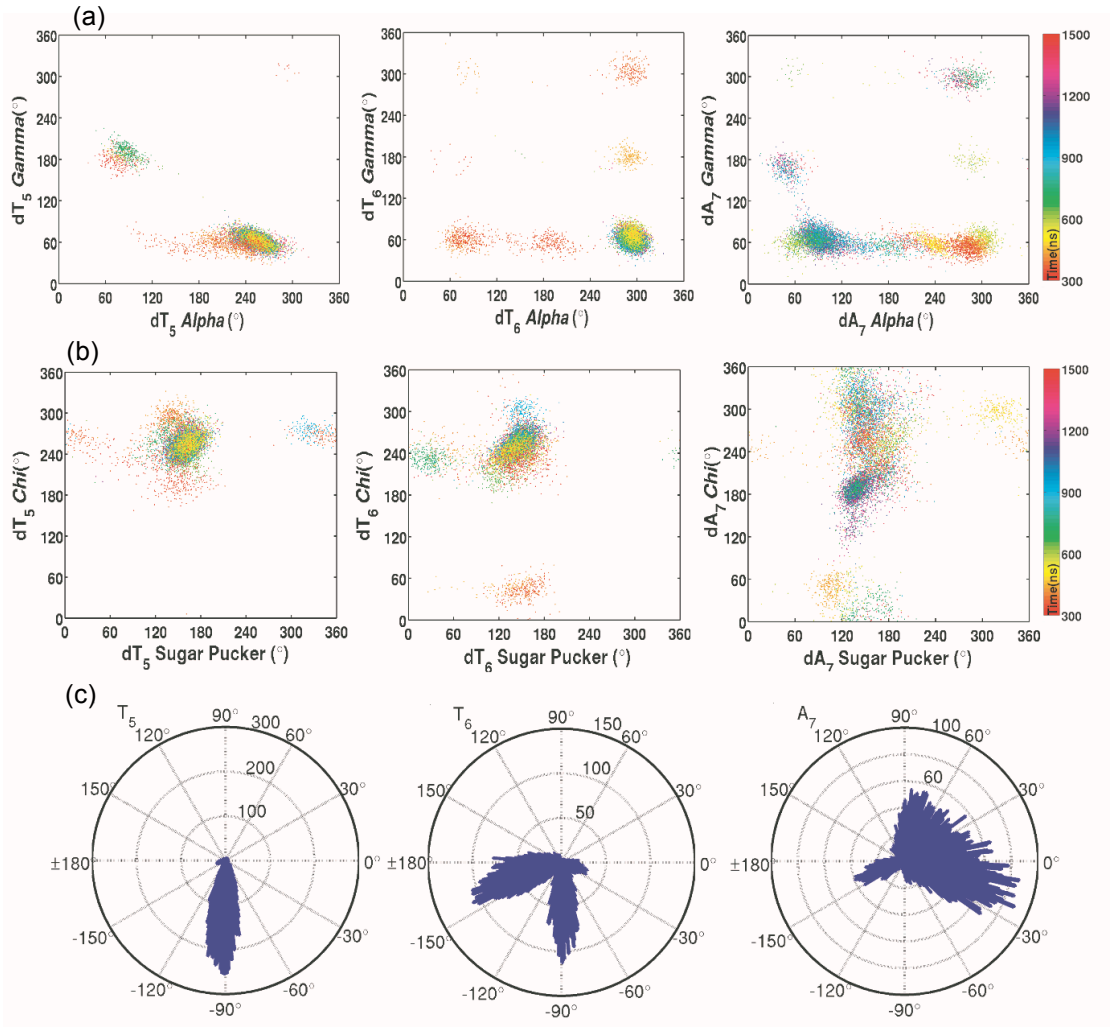

Figure S6: Representation of **(a)** α/γ torsion angle **(b)** χ vs pucker and **(c)** Angular histogram of B_I/B_{II} parameter for loop1 (Thy5, Thy6, Ade7). The backbone torsion angle parameters are not constrained and highlight the flexibility of loop1. The glycosidic χ-angle of Ade7 is in *syn* conformation when it interacts with A1:A13 base pair to form a triad. The α/γ torsions and B_I/B_{II} sampling of Ade7 highlight that it occupies non canonical conformations in triad formation. Therefore triad formation is a transient event, lasting for 40 ns due to the constraints put by the distortions in the backbone angles.

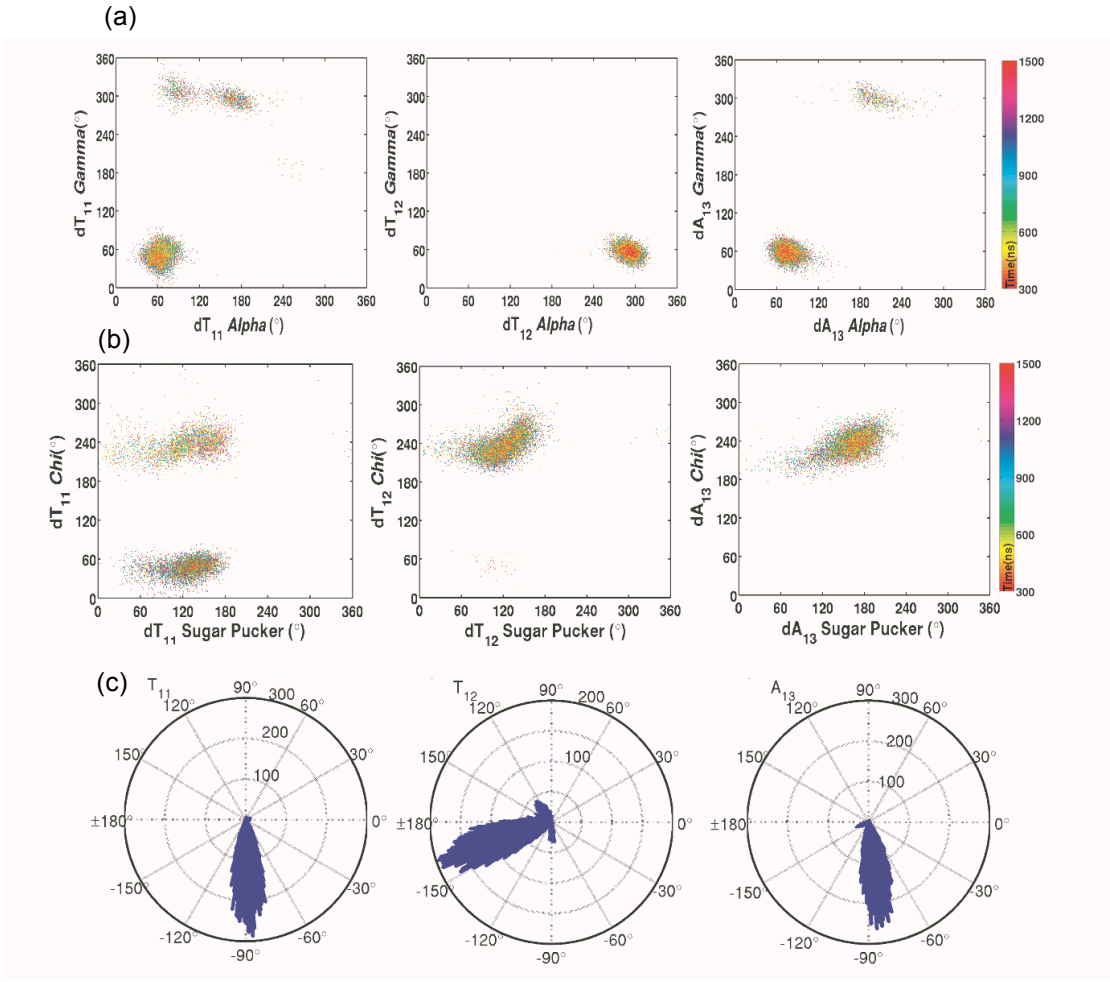

Figure: S7 Representation of **(a)** α/γ torsion angle **(b)** χ vs pucker and **(c)** angular histogram of B_I/B_{II} parameter for loop2 (Thy11, Thy12, Ade13). The α/γ angles of Thy11 and Ade13 lie in non-canonical regions but the base continues to stay in energetically favourable B_I conformation.

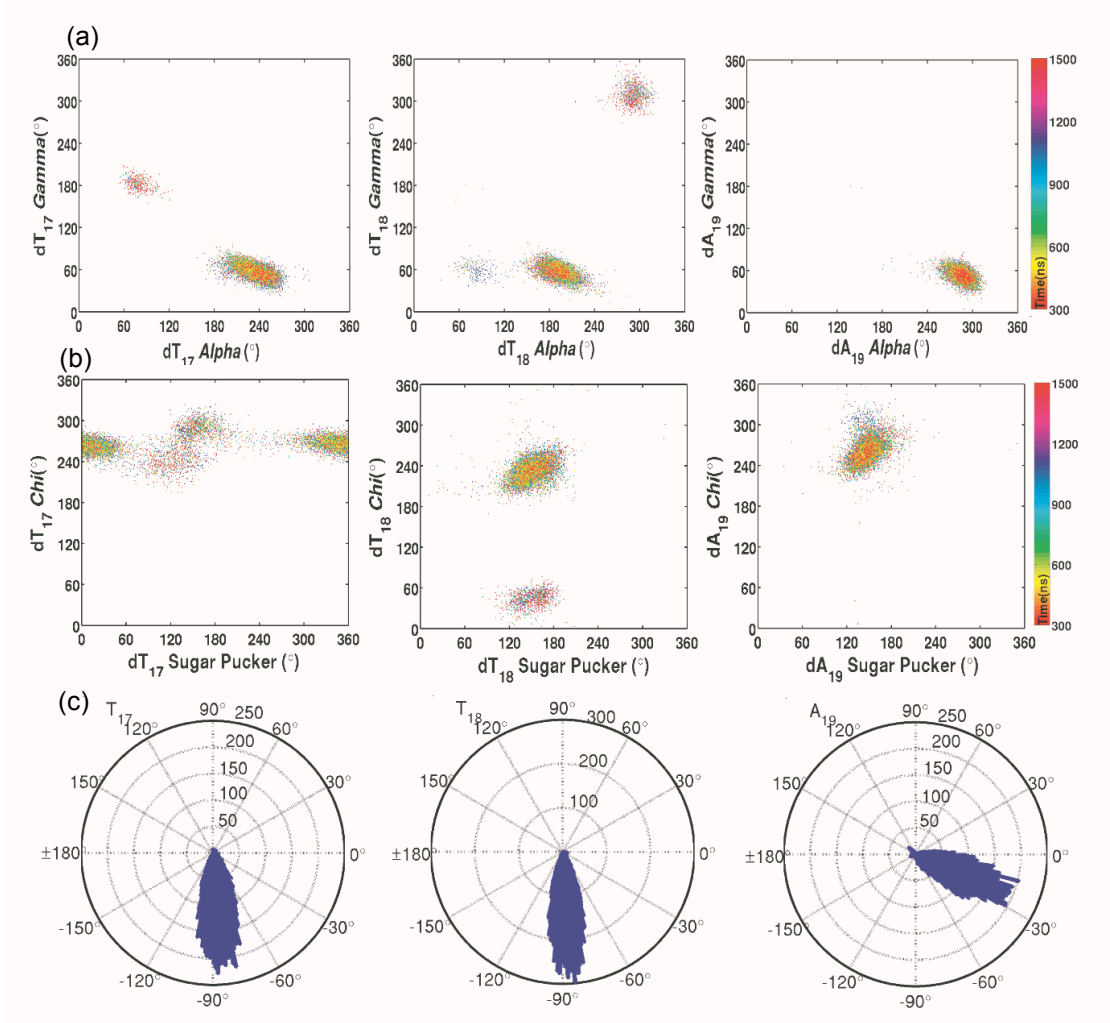

Figure S8: Representation of **(a)** α/γ torsion angle **(b)** χ vs pucker and **(c)** angular histogram of B_I/B_{II} parameter for loop3 (Thy17, Thy18, Ade19). The sugar pucker of Thy17 is in C3'-*endo* conformation to facilitate interaction with Gua15 to form pentad. The α/γ angle of Thy18 is pushed in t/g+ conformation due to alignment of Thy17 with the middle quartet.

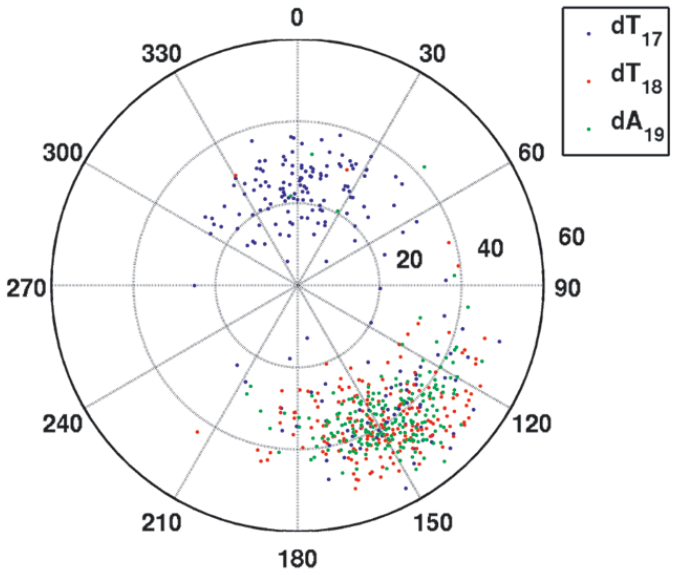

Figure S9: Polar plot showing sugar puckering of bases in loop3. Thy17 occupy C3'-*endo* conformation while Thy18 and Ade19 occupy C2'-*endo* conformation

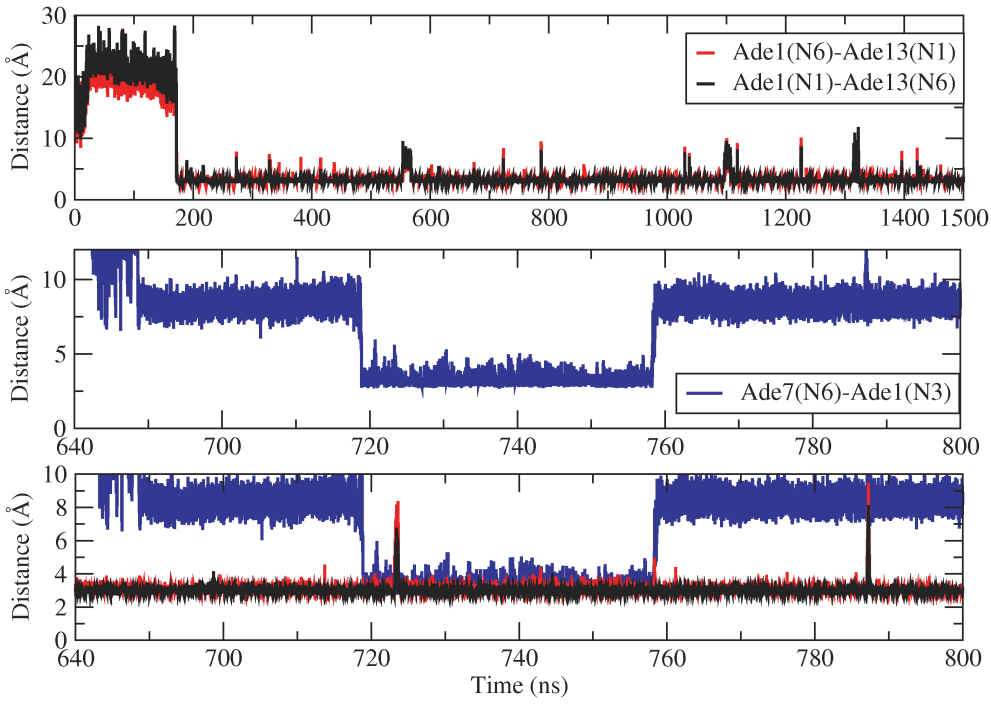

Figure S10: A1:A13 base pair and A1:A7:A13 triad formation supported by minimum distance sampling over the course of simulation. **(top)** The A:A base pair is formed around 180ns and last the entire simulation time. (middle) Interactions of Ade7 and Ade1 results in the formation of a A:A:A triad. **(bottom)** The Triad is formed ~720ns and lasts for only ~40ns due to the unfavourable conformation of the backbone torsion angles.

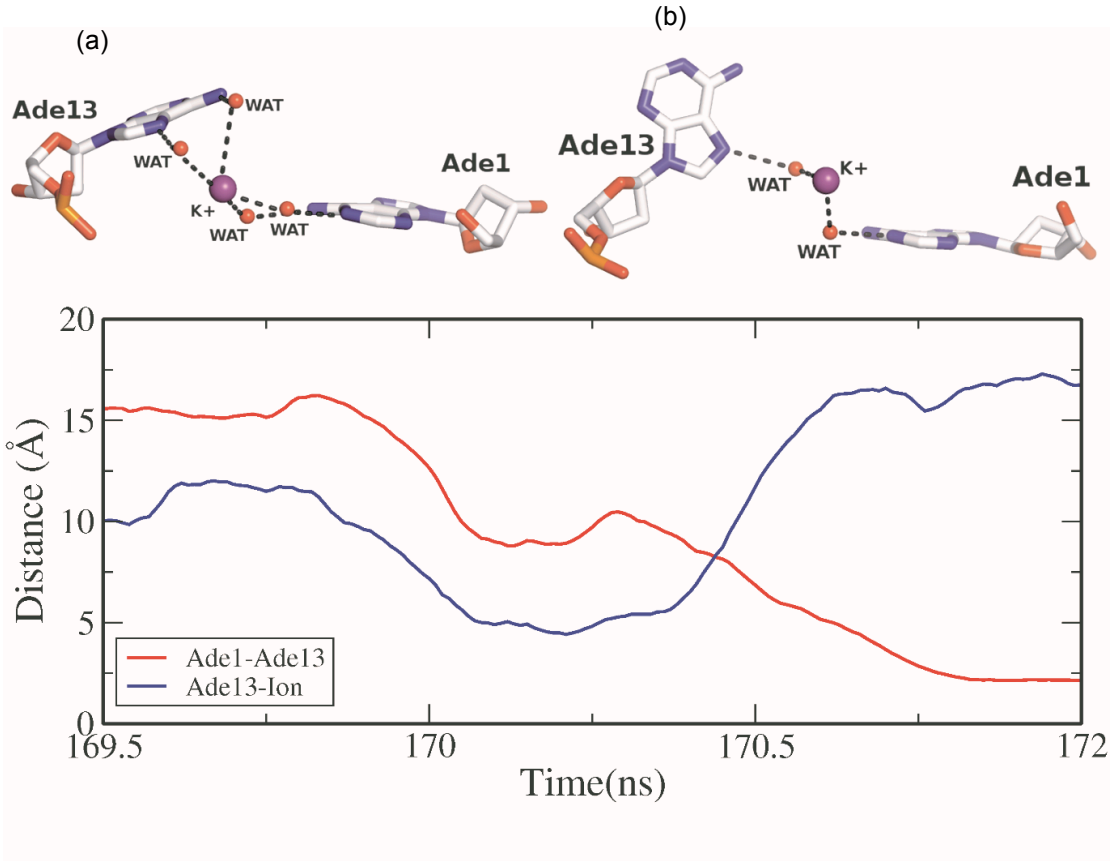

Figure S11: The role of K+ ions in stabilisation of A:A base pair formation. **(a,b)** Ade1 and Ade13 interact with K+ ion via its hydration shell. The dispersion of the ion is linked with the formation of the stable A:A base pairing. **(c)** A plot of minimum distance between Ade13-K^+ ion (blue) and Ade1 and Ade13 (red) highlights the presence of the K+ ion meadiating Ade1 and Ade13 interactions..

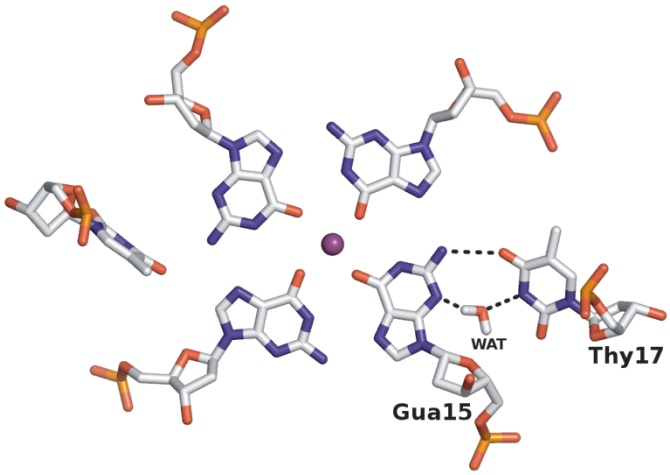

Figure S12: Role of solvent in bridging the interaction of Thy17 with Gua15. The O4 of Thy15 can hydrogen bond directly with N2 of Gua15. However, the N3 of Thy17 is not within hydrogen bonding distance of N3 of Gua15 and interacts via a water bridge.

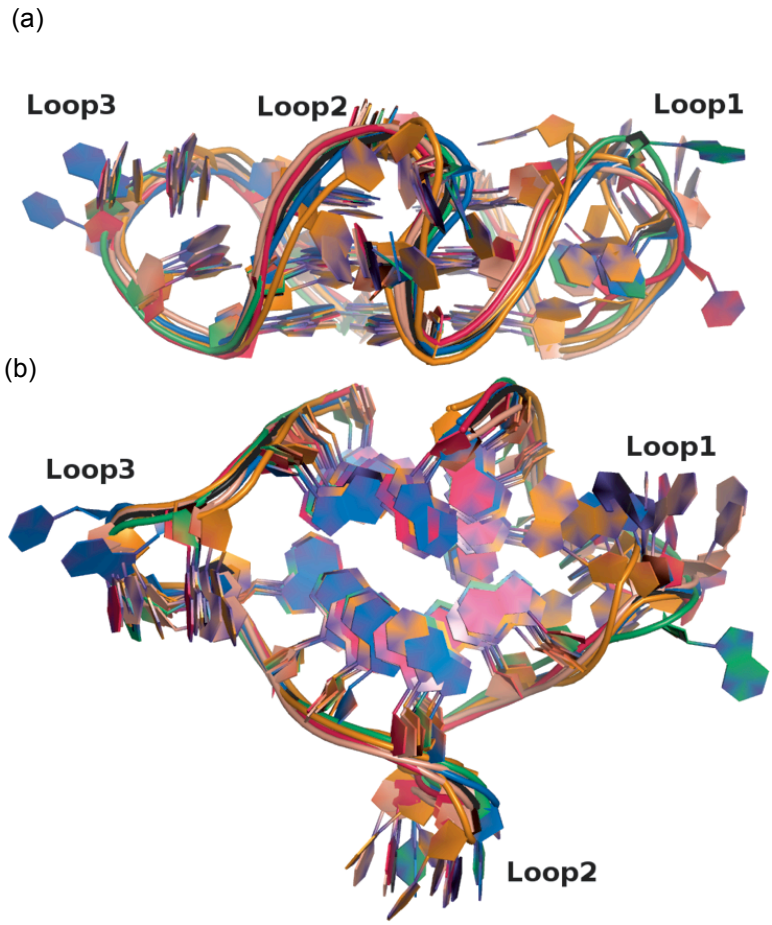

Figure S13: Polymorphism of human parallel stranded propeller-type quadruplex observed during the simulation. A conformation representative of cluster was extracted from clustering analysis done after initial equilibration. **(a)** Side and **(b)** Top view of the conformers are shown. The figure highlights that the loops are the most flexible regions in the structure..

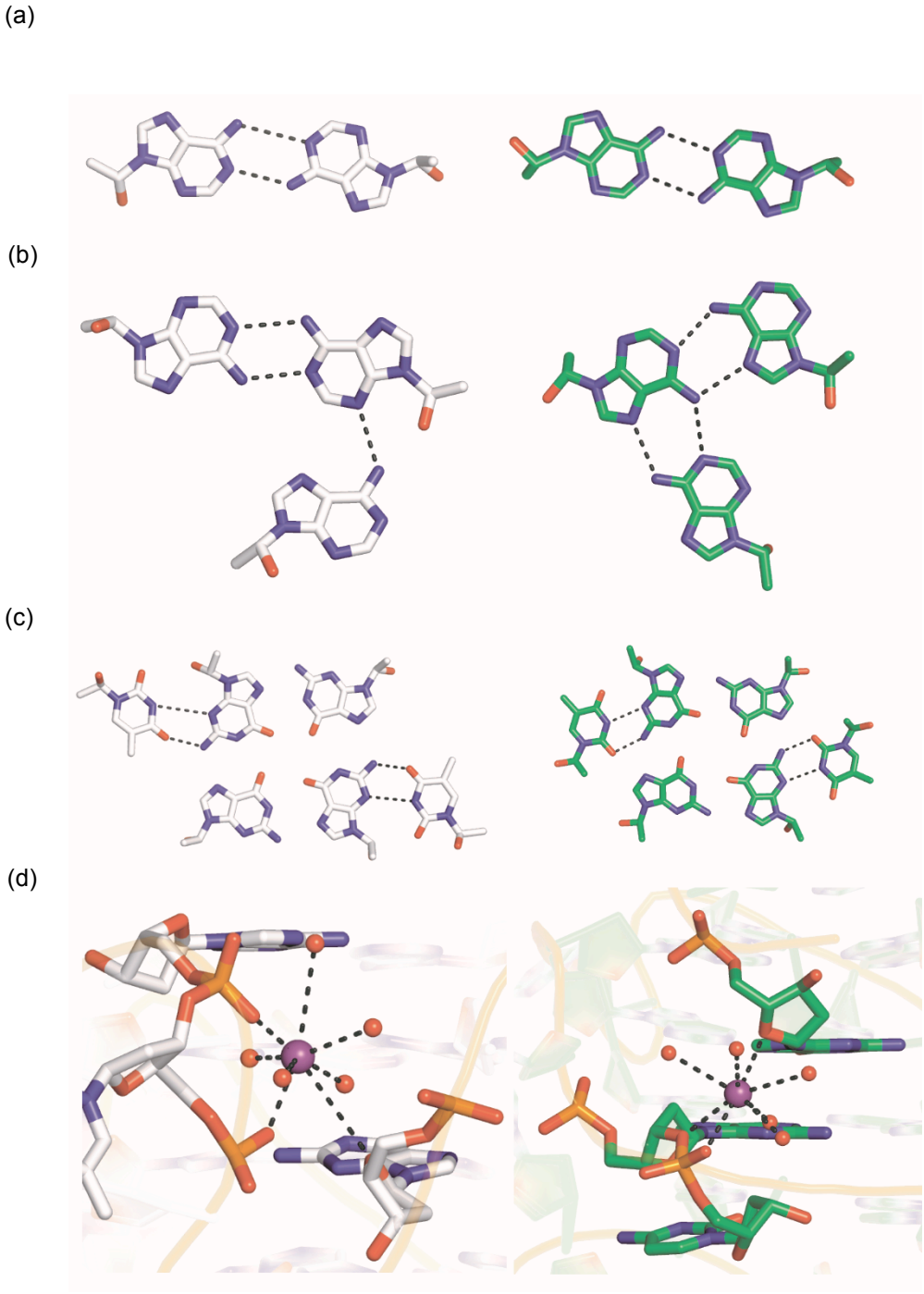

Figure S14: Comparison of the simulation **(left)** with the the experiment **(right)**. Conformational similarity identified in the simulation with **(a)** A:A base pair (PDB id 1LNG) **(b)** A:A:A triad (PDB id 1FJG) **(c)** T:(GGGG):T hexad (PDB id 1XCE) and (d) role of ion in the stabilisation of the loop in the quadruplex of c-kit promoter (PDB id 3QXR).